

In the Matter of Entropy Nuclear Vermont Yankee LLC

Docket No. 50-271 Official Exhibit No. NEC-JH-40

NEC-JH_40

OFFICE SECTION

OFFERED by: Applicant/Licensee Entropy Nuclear Vermont Yankee LLC Intervenor NEC

NRC Staff Other

IDENTIFIED on 7/23/08 Witness/Panel Hopewald

Action Taken: ADMITTED REJECTED WITHDRAWN

Reporter/Clerk MAC

A New Approach for Investigation of Erosion-Corrosion Using Local Flow Models

Y.M. Ferng, Y.P. Ma, K.T. Ma,* and N.M. Chung**

DOCKETED
USNRC

August 12, 2008 (11:00am)

OFFICE OF SECRETARY
RULEMAKINGS AND
ADJUDICATIONS STAFF

ABSTRACT

Erosion-corrosion (EC) is a piping degradation mechanism that causes material loss from the inside of piping and thinning of the wall. EC is believed to be a coupled phenomenon including chemical corrosion and mechanical erosion, which is dominated by piping layout, fitting geometry, and local flow structure. A new approach was proposed for investigation of EC phenomenon using local flow models, including the multidimensional, two-fluid model to simulate flow characteristics within piping and EC models to predict two-dimensional distributions of EC locations. Impacts of gravitational and centrifugal forces on two-phase flow behaviors were captured reasonably well by the current three-dimensional, two-fluid models. EC locations predicted by the proposed models showed satisfactory agreement with distributions of wear sites measured in practice. Results showed the models explained the EC phenomenon reasonably well.

KEY WORDS: elbows, erosion-corrosion, ferrous ions, flow, hydrodynamics, impingement, mechanical erosion, modeling, nuclear applications and environments, pipelines, reducers, etc.

INTRODUCTION

Erosion-corrosion (EC) is a piping wear mechanism that causes material loss from the inside of pipes and subsequent wall thinning. It is a crucial problem in

piping systems for nuclear or fossil fuel power plants since it may force costly repairs and cause injuries. Essentially, this wear is dominated by two major mechanisms: chemical corrosion, including chemical oxidation near the wall and dissolution of its products, and mechanical erosion accelerated by fluid flowing inside the pipe or high-velocity liquid droplets impinging on the oxidized pipe wall. The EC phenomenon depends strongly upon piping layout, fitting geometry, local distributions of flow properties, and flow chemistry.

Previous research into the EC phenomenon has concentrated mostly on prediction of the wear rate. These efforts have included development of the CHEC¹ code,¹ CEACE¹ code,² KWU (Kraftwerkstechnik) correlation,³ EdF (Electricité de France) model,⁴ MIT (Massachusetts Institute of Technology) model,⁵ and the hydrodynamic EC model.⁶⁻¹¹ Except for the hydraulic model,⁶⁻¹¹ these models evaluate the global wear rate of piping and can be considered as zero-dimensional models. The models presented by Nesic and Postlethwaite, et al., are localized models that essentially are derived from local flow structure and can be used to calculate the one-dimensional distribution of the wear rate.¹¹⁻¹²

During the outage of the Maanshan nuclear power plant (MNPP) in Taiwan, wall thickness data as measured by an ultrasonic transmitter (UT) showed distributions of EC locations on the pipe wall displayed a two-dimensional behavior. The data were influenced strongly by upstream fittings and external forces, including centrifugal and gravitational forces. Previous models cannot capture these multidimen-

Submitted for publication July 1997; in revised form, January 1998.
*Institute of Nuclear Energy Research, P.O. Box 3-3 Lung-tan, 325, Taichung, Taiwan, R.O.C.
**Power Research Institute, Taiwan Power Co., 84 Ta-An Road, Taichung, R.O.C.
*Trade name.

CORROSION

LOC
pipi:
mode
expla
local
the pi
remov
erosio

LOC

Hydr
The
one co
one tw
energy
tutive n
and app
conditic
In t
made in
tive equ
- N
liquid an
- Pi
- Th
and set a
- Th
is selecte
- Th
phase flow
turbulenc
model of t

sional characteristics and simulate the dependence of piping layout.

The present work focused on qualitatively investigating the multidimensional characteristic of EC phenomenon using local flow models to predict the multidimensional distributions of wear sites. The three-dimensional hydrodynamic model then was used to calculate the single- or two-phase flow structures, and EC models were used to predict the distributions of EC locations. The piping selected in the current simulation was located in the extraction and exhaust systems of high-pressure turbines (HPTB) within MNPP since most of the serious EC at the plant occurs there, based upon plant-measured wall thickness data. The current hydrodynamic model reasonably simulated flow characteristics governed by piping layout, centrifugal force, and gravitational force. Predicted distributions of EC locations by the current EC models coupling with local flow structures corresponded well with the plant-measured data. This agreement revealed that the proposed local flow models, including the hydrodynamic and EC models, could be used to explain EC occurring at fittings within MNPP.

LOCAL FLOW MODELS

The multidimensional flow structure within the piping was obtained using current hydrodynamic models. The major phenomenon for EC wear could be explained by the presented EC models, coupled with local flow characteristics. The EC models included the production of oxides for corrosion and oxide removal, as well as liquid droplet impingement for erosion.

Hydrodynamic Models

The hydrodynamic models studied consisted of one continuity equation, one momentum equation, one two-equation turbulent model (turbulent kinetic energy [k] – the energy dissipation rate [ε]),¹² constitutive models for interphase exchange phenomena, and appropriate numerical scheme and boundary conditions.

In these models, the following assumptions are made in deriving the governing equations, constitutive equations, and appropriate boundary conditions:

- No heat transfer or mass transfer between liquid and vapor phases is considered;
- Pressure is the same for both phases;
- The diameter of the liquid droplet is constant and set at 1.0 mm;
- The particle form of the interphase drag force is selected for the liquid droplet flow;
- The standard k – ε turbulent model for single-phase flow is adopted. The effect of bubble-induced turbulence is taken into account in the turbulent model of two-phase flow;

– The pipe length at the outlet side is long enough that fully developed flow can be assumed; and

– Since the steam quality in the simulated pipe systems is ~ 88% to 92%, the two-phase flow can be considered droplet flow.

The continuity governing equation is derived as:

$$\nabla \cdot (\alpha \rho_i \bar{u}_i) = 0 \quad (1)$$

where u is velocity, α is the volumetric fraction of each phase, and $i = c$ for continuous vapor and d for dispersed liquid droplet.

The momentum equation is derived as:

$$\nabla \cdot (\rho_i \alpha_i \bar{u}_i \bar{u}_i) = -\alpha_i \nabla P + \nabla \cdot \left[\alpha_i (\mu_{i,c} + \mu_{i,t}) \nabla \bar{u}_i \right] + \bar{S}_{u,i} \quad (2)$$

where $\mu_{i,c}$ is the molecular viscosity, $\mu_{i,t}$ is the turbulent viscosity, $\bar{S}_{u,i}$ is the source term due to gravitational force and interphase drag, P is pressure, and ρ is density.

Turbulent Model – In the current model, the turbulent model for two-phase droplet flow essentially adopts the well-known k – ε two-equation model of the single phase. The turbulent shear stress for the continuous phase can be expressed by the Boussinesq concept:¹³

$$-\rho \overline{u'v'} = \mu_t \frac{\partial u}{\partial n} \quad (3)$$

where u' and v' are velocity fluctuations, and n is the distance normal to the wall. Similarly, the turbulent viscosity (μ_t) can be evaluated by the traditional k – ε model:

$$\mu_t = c_\mu \frac{k^2}{\varepsilon} \quad (4)$$

where c_μ is the turbulent model constant. Both parameters k and ε can be obtained by solving the transport equations:

$$\nabla \cdot (\rho \alpha_i \bar{u}_i \phi) = \nabla \cdot \left[\rho \alpha_i \left(\mu_{i,c} + \frac{\mu_{i,t}}{\sigma_\phi} \nabla \phi \right) \right] + \rho \alpha_i (P_\phi - \varepsilon) + S_{p,\phi} \quad (5)$$

where $\phi = k$, the turbulent kinetic energy = ε , the turbulent energy dissipation rate, P_ϕ , the turbulent generation term, has the same expression as the standard k – ε two-equation model.

Additional source $S_{p,\phi}$ is used to take into account the enhanced effect on turbulence of the continuous phase caused by droplet agitation. Based

upon the modified formula of Mostafa and Mongia, this source can be described as:¹⁴

$$S_{p,k} = \frac{2\rho_d \alpha_c \alpha_d k}{\tau_p} \left(1 - \frac{\tau_c}{\tau_c + \tau_p} \right) \quad (6)$$

$$S_{p,t} = \frac{-2C_{t3} \rho_d \alpha_c \alpha_d \epsilon}{\tau_p} \left(1 - \frac{\tau_c}{\tau_c + \tau_p} \right) \quad (7)$$

where C_{t3} is the turbulent model constant, and τ_c is the time scale characterizing large-scale turbulent motion:

$$\tau_c = 0.34 \frac{k}{\epsilon} \quad (8)$$

where τ_p is the time scale characterizing the droplet response:

$$\tau_p = \frac{4 D_b \rho_d}{3 C_d \rho_c} \frac{1}{|\bar{u}_c - \bar{u}_d|} \quad (9)$$

where D_b is the droplet diameter, and C_d is the drag coefficient and has the following correlations as proposed by Cliff, et al.:¹⁵

$$C_d = \begin{cases} 24.0 \frac{(1.0 + 0.15 Re^{0.687})}{Re} + \frac{0.42}{(1.0 + 4.25 \times 10^5 Re^{-1.16})} & Re \leq 3.38 \times 10^5 \\ 29.78 - 5.3 \log_{10}(Re) & 3.38 \times 10^5 < Re \leq 4 \times 10^5 \\ 0.1 \log_{10}(Re) - 0.49 & 4 \times 10^5 < Re \leq 10^6 \\ 0.19 - \frac{8 \times 10^4}{Re} & Re > 10^6 \end{cases} \quad (10)$$

Constitutive Equations — The constitutive equations that account for interactions between the two phases include:

Void fraction:

$$\alpha_c + \alpha_d = 1 \quad (11)$$

Momentum exchange between the two phases:

$$\bar{F}_d = -\bar{F}_c \quad (12)$$

$$\bar{F}_c = f_{int} (\bar{u}_c - \bar{u}_d) \quad (13)$$

where F_d and F_c are the interphase drag forces for both the dispersoid and continuous phases, and f_{int} is the interphase friction factor between the vapor and liquid phases. The total drag force per unit volume can be evaluated as the sum of the drag forces on each individual spherical droplet contained in that volume. Then, f_{int} can be expressed as:

$$f_{int} = \frac{3 \rho_c \alpha_c C_d}{4 D_b} |\bar{u}_c - \bar{u}_d| \quad (14)$$

Numerical Scheme — Three-dimensional, two-fluid equations are used to calculate the flow characteristics in the piping to simulate the EC phenomenon through the use of calculated local flow distributions. Since the geometry of the simulated pipe is not that of a simple rectangular or cylindrical system, a body-fitted coordinate (BFC) method is adopted to deal with this multidimensional geometry.¹⁶ The differential equations are discretized using a control volume approach in a finite-difference form. The details of the control volume approach for the finite-difference method have been described previously.¹⁷ The hybrid scheme is used to treat the convection terms coupled with the diffusion terms. The coupled equations for the velocity and pressure are solved by the interphase slip algorithm (IPSA),¹⁸ which is a two-phase extension of the well-known SIMPLE (semi-implicit method for pressure-linked equations) scheme for single-phase flow.¹⁹ The optimum false time (Δt_{false}) is used throughout the steady-state calculation and can be given by the Courant criterion as:

$$\Delta t_{false} = \frac{\Delta X}{U} = 1 \quad (15)$$

where ΔX is a characteristic length in the computation domain, and U is a characteristic velocity.

The procedure in solving this three-dimensional, two-phase model is:

- Step 1: Set the boundary conditions on the solution domain based upon the plant data.
- Step 2: Solve the momentum equations for the velocities of both phases,
- Step 3: Solve the pressure correction equation based on the joint continuity equation to eliminate the mass conservation error,
- Step 4: Correct the velocities and update the pressure.
- Step 5: Solve the continuity equations for the volume fractions.

th
vi:
co
to
PF
co
Mc
HF
tio
inc
ph:
ph:
car
dor
are
Sin
nea
the
nee
EC
are
sior
ste
into
on t
wher
solu
with
cent
whic
wher
the s
I
shou
Then

— Step 6: Solve the $k - \epsilon$ equations to obtain the turbulent characteristics and update turbulent viscosity, and

— Step 7: Repeat Steps 2 through 6 until the convergent criteria are satisfied.

Several computational flow codes can be applied to solve this problem, including TEACH,^{1,20} PHOENICS,^{1,21} and FLOW3D,^{1,22} etc. The PHOENICS code was selected in the current calculation work. Most of the calculation works were performed on an HP-750¹ workstation.

Boundary Conditions — Inlet boundary conditions are set based upon the plant conditions, which include the velocities and volume fractions of both phases. A very long pipe is added to the outlet of the physical domain so that fully developed conditions can be reached at the outlet of the calculational domain. Then, no special outlet boundary conditions are specified, except for a fixed system pressure. Since the turbulent flow behaviors change abruptly near the wall, the wall function method is adopted for the velocity and turbulent distributions to avoid the need for finer grids near the wall.²³

EC Models

The EC models in the current study essentially are divided into two major parts: the chemical corrosion model and the mechanical erosion model.

Basic EC Model — The basic EC model of carbon steel in a fully developed pipe flow can be divided into two parts:⁴

The first is the dissolution rate (R_p) of magnetite on the metal surface:

$$R_p = 2k_R(C_{eq} - C_w) \quad (16)$$

where k_R is the reaction-rate constant, C_{eq} is the soluble ferrous ion (Fe^{2+}) concentration at equilibrium with the magnetite, and C_w is the soluble Fe^{2+} concentration at the oxide water interface.

The second is the mass-transfer rate of Fe^{2+} , which can be modeled as:

$$R_c = \kappa_m(C - C_\infty) \quad (17)$$

where κ_m is the mass-transfer coefficient and C_∞ is the soluble Fe^{2+} concentration at the bulk water.

For steady-state, fully developed pipe flow, R_p should be equal to the mass-transfer rate of Fe^{2+} (R_c). Then, the total metal loss rate can be expressed as:

$$R = \frac{C_{eq} - C_\infty}{\frac{1}{2k_R} + \frac{1}{\kappa_m}} \quad (18)$$

Local EC Model — Local corrosion reactions include the electrochemical reaction, the precipitation reaction, and the chemical oxidation. The total reactions reasonably can be assumed to be completed at the pipe wall, while none of the iron ions produced in the electrochemical reaction are transported across the boundary layer prior to the subsequent chemical oxidation. The local EC rate then can be assumed to be dominated by the local oxide production rate and its transfer rate. According to experimental observation, the local corrosion production rate is proportional to the difference in the soluble Fe^{2+} concentration between the wall and the oxide.⁴ In other words, the steeper the near-wall radial profile of concentration is, the higher the wear rate is. The concentration of soluble Fe^{2+} at the equilibrium with the magnetite depends upon the temperature of the solution and the concentration of the chemical agent. Lower local near-wall fluid velocity will cause lower concentrations of the chemical agent, such as pH value or dissolved oxygen, enhance the local corrosion production rate, increase the gradient of soluble Fe^{2+} concentration, and consequently promote metal loss of the pipe wall. Therefore, lower near-wall fluid velocity is a good indicator to express the possible distributions of EC locations.

In addition, the local mass-transfer rate of Fe^{2+} also may influence the corrosion rate. This transfer rate generally is governed by the mass transfer of Fe^{2+} near the pipe wall.^{4,6-7} As described above, κ_m can be expressed in an analogy to the Dittus Boelter's equation:

$$\kappa_m \propto \frac{ShXD_{diff}}{d} \quad (19)$$

where $Sh = a_1 Re^{a_2} Sc^{a_3}$, and:

$$Re = \frac{\rho Ud}{\mu} \quad (20)$$

$$Sc = \frac{D_{diff}}{\mu} \quad (21)$$

and where d is the pipe diameter; D_{diff} is the diffusivity of soluble ion; μ is the viscosity; U is the characteristic velocity; ρ is the fluid density; and a_1 , a_2 , and a_3 are constants.

The local EC rate is governed by this mass-controlled phenomenon,^{6,7,11} which is proportional to its coefficient (Equation [17]). According to this equation, higher local velocity results in higher mass-transfer coefficients (κ_m), subsequently causing higher wear rates. In other words, high local velocity of flowing flow is an effective mechanism to remove Fe^{2+} near the pipe wall, which may enhance EC.

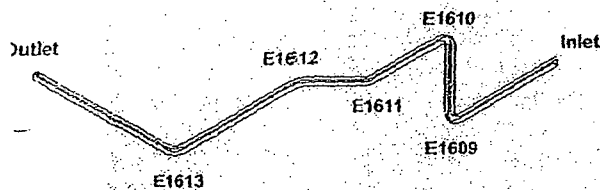


FIGURE 1. Schematic of pipe layout.

Then, the higher near-wall velocity may be a parameter to indicate possible wear sites.

The major task of the current work was to investigate the EC phenomenon by finding the possible distributions of wear sites using local flow models. Then, the qualitative indicators to express the wear patterns but not quantitative calculations to evaluate the wear rate, were adopted. In addition, the model using the indicator of lower velocity to simulate EC governed by Fe^{2+} production is called the production model, and the model using the parameter of higher velocity to describe the EC dominated by the Fe^{2+} transfer rate is called the transfer model.

Droplet Impingement Model— The simulated system in this work is a wet steam system with flow quality of 85% to 92%. This high-quality flow system can be considered as a droplet flow system in which the size of the liquid droplet is sufficiently small, and the droplet can be carried by the high-velocity steam. A liquid droplet with enough high kinetic energy can impinge the oxide layer of the metal and erode it on the pipe wall surface, enhancing EC. This kind of damage on the oxide layer is known as droplet impingement or liquid impact erosion that also dominates EC wear.

Many parameters affect the complicated droplet impingement. A model simply describes the phenomenon as one where the oxide layer caused by erosion is removed by the action of numerous individual impacts of liquid droplets.⁴ Its form can be expressed as:

$$m = C_s N F_0(\theta) \frac{\rho_l U_n^2}{HV} \quad (22)$$

m is the wear rate. C_s is a system constant determined by fabrication and installation of piping, a representation of frequency. F_0 is a characteristic function. θ is the angle of impact, ρ_l is the liquid density, U_n is the normal velocity, and HV is the hardness of the pipe wall. Equation (22) shows that the metal loss from droplet impact is proportional to the concentration of liquid droplet and its normal velocity. Then, the erosion rate reasonably can be considered to be associated with the erodent kinetic energy that can be expressed simply as $\alpha_r U_n |U_n|$,

which is a good parameter to indicate wear sites. In this form, α_r is the volume fraction of the liquid droplet, and U_n is its corresponding velocity in the normal direction toward the wall.

RESULTS AND DISCUSSION

A new approach is proposed to simulate the EC phenomenon through local flow models. This approach includes the multidimensional, two-fluid models and the EC models. The simulated pipes are located at the extraction and exhaust systems of HPTB within MNPP. In these systems, the quality of two-phase flow is ~ 88% to 92%, implying that the two-phase flow characteristic can be considered as droplet flow. The models including the droplet form of two-fluid equations and the erosion model due to droplet impingement can be applied in these systems.

HPTB Exhaust System

The simulated pipe in this system is a steam line of 14 in. (0.36 m) connecting HPTB and Feedwater Heater (FWHR) No. 2. This pipe is shown schematically in Figure 1 and consisted of two vertical elbows of 90° (Elbows E1609 and E1610), one horizontal elbow of 90° (Elbow E1613), and two horizontal elbows of 45° (Elbows E1611 and E1612). The flow properties within this pipe are that the system pressure is 199.7 psia (1.38 MPa), temperature is 382°F (467.6 K), quality is 88.6%, and mass flow rate is 263,152 lb/h (33.16 kg/s).

Figure 2 displays the liquid fraction distributions near the wall within this pipe, while the right part shows the liquid fraction distributed in Elbows E1609 and E1610. The left part shows the liquid fraction distributed in Elbows E1611 to E1613. Since three-dimensional results cannot be shown appropriately in a two-dimensional plane, only the liquid fraction distributions near the inner and outer sides of the elbow are shown. The scale on the right side of the figure represents the liquid fraction. As the two-phase mixture horizontally flows through Elbow E1609 and then turns to flow upward along the vertical pipe, the centrifugal force will push the heavier liquid droplet to the outer side of the elbow, causing more liquid to be accumulated there. The phenomenon that centrifugal force governs the liquid droplet behavior is shown clearly in the right portion of Figure 2. The yellow region located at the outer side of Elbow E1609 represents higher liquid fraction, and the blue region representing lower liquid fraction is shown at the inner side of the elbow. As the droplet flow passes upward through Elbow E1610 and turns to the horizontal direction, the centrifugal effect also demonstrates in the plot of liquid fraction distribution. The direction of centrifugal force points upward and is opposite to that of the gravitational force

pointing to the outer side. The more liquid accumulation phenomenon overcomes the elbow and droplet exit. The liquid fraction distribution is because of centrifugal force. The result can be liquid fractionally changes: the lower part of the pipe connects to a horizontal left and right part of Figure 2. The distribution region is shown through and after the liquid fraction distributions of flow parameters. The prediction of EC location and the prediction of the piping are plant measurements are derived from the smooth

⁴ Electric Power Research Institute, Report No. CA-94304-1395.

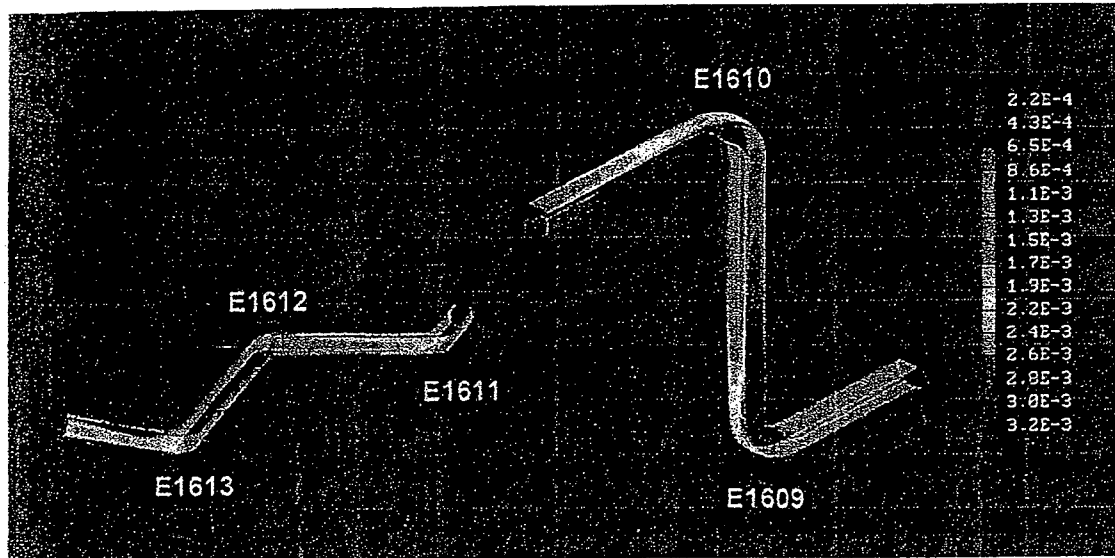


FIGURE 2. Near-wall distribution of liquid fraction.

pointing downward. The yellow-red region appears at the outer and upper side of Elbow E1610, indicating more liquid droplets accumulated there. This phenomenon demonstrates that the centrifugal force overcomes the gravitational force within the vertical elbow and then dominates the behavior of liquid droplet existing in the two-phase mixture.

The liquid droplet gradually will fall down, because of the downward gravitational force as the fluid continues to flow along the horizontal pipe. This result can be confirmed at the right portion of the liquid fraction plot in which the upper region gradually changes from yellow to green and, in contrast, the lower part changes from deep blue to blue. Since the pipe connecting Elbows E1611 to E1613 belongs to a horizontal pipe, the liquid fraction located at the left and right sides of the elbow is shown in the left part of Figure 2. The centrifugal force again governs the distribution of liquid phase so that the yellow region is shown at the outer sides of Elbows E1611 through and E1613, respectively.

After the three-dimensional two-phase characteristics have been obtained, it was crucial to find the distributions of wear sites from these calculated local flow parameters. Figures 3 and 4 show the comparison of EC locations between the plant measured data and the predicted results for Elbows E1610 and E1613, respectively, since only these elbows within the piping are measured by the plant staff. These plant measured data are the severe wear sites, which are derived from the raw data of pipe wall thickness by the smoothing method), as suggested by the Elec-

tric Power Research Institute (EPRI).⁽¹⁾ Wall thickness is measured by the UT during the plant outage period. These figures are the two-dimensional plots for the distributions of EC locations, which are plotted by cutting the elbows from the outer side. Then, the lower and upper parts of these two-dimensional plots represent the outer side of the elbow, and the central part indicates the inner side of the elbow. In the plots, the blacker the color is, the more severe the EC damage is. Plot (a) in Figures 3 and 4 is the distributions of EC locations measured by the plant staff, while Plot (b) is the distributions predicted by the liquid droplet impingement model. Plot (c) is the distribution predicted by the Fe^{2+} production model, and Plot (d) is predicted by its transfer model.

Since Elbow E1610 is located at the same plane with the upstream elbow and inlet, the flow behavior may display symmetry characteristics, which induce the symmetry pattern of EC wear. This phenomenon is shown in the measured data as well as the predicted results (Figure 3). In Plot (a) of Figure 3, the blacker regions are located at the upper-right and lower-right corners of the two-dimensional plots. The measured wear pattern of Elbow E1610 reveals that the serious EC is distributed on the outer and downstream location of the elbow. The calculated results of Plots (b) and (c) correspond with the measured wear locations, and Plot (d) predicted results cannot match the measurement. These comparisons clearly show that EC occurring at Elbow E1610 essentially is dominated by the liquid droplet impingement and the Fe^{2+} production effect based on the current EC models. A similar result is displayed in the EC phenomenon occurring at Elbow E1613 (Figure 4). The measured data shows the wear sites mostly are

⁽¹⁾ Electric Power Research Institute, 3412 Hillview Ave., Palo Alto, CA 94304-1395.

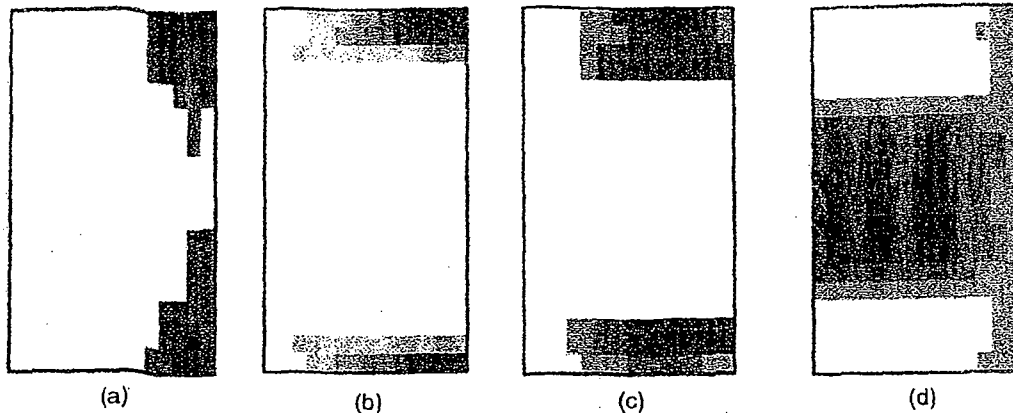


FIGURE 3. Comparison of wear sites for Elbow E1610.

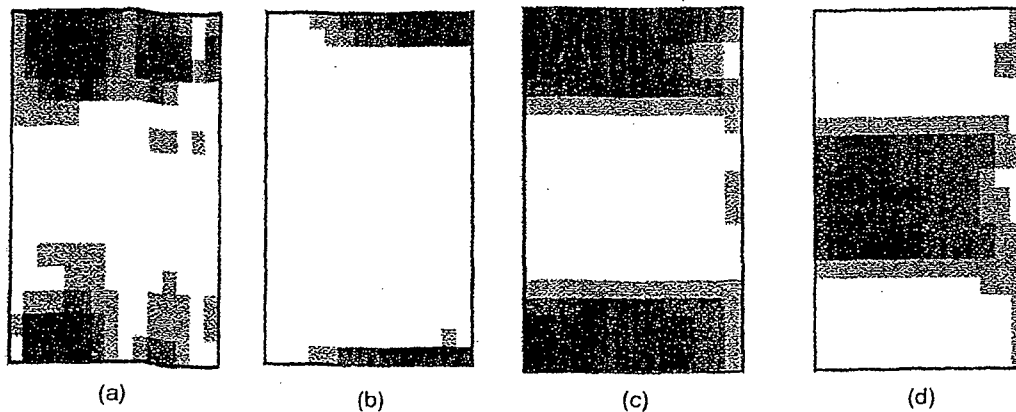


FIGURE 4. Comparison of wear sites for Elbow E1613.

located at the outer side of the elbow (i.e., the black regions near the upper and lower sides of EC location plot), which is captured qualitatively by the droplet impingement and oxide generation models. The corrosion model dominated by Fe^{2+} transfer predicts the various EC distributed around the central portion of the two-dimensional plot (i.e., the inner side of Elbow E1613), which does not agree with the measured data. The EC phenomenon occurring at the horizontal elbow (Elbow E1613) can be explained to be caused by the droplet impingement and Fe^{2+} production effect, based upon the qualitative agreement in the two-dimensional wear pattern between the model prediction and plant measurement.

HPTB Extraction System

The HPTB extraction system is a steam system connecting the HPTB and FWHR 1, in which the flow properties are that the system pressure is 413.7 psia (28.15 MPa), temperature is 447.9°F (504.2 K), quality is 92%, and mass flow rate is 382,331 lb/h (173,800 kg/s). The simulated pipe located in this

system includes two horizontal elbows of 16 in. (0.41 m, Elbows E1829 and E1830), one horizontal reducer of 16 in. to 14 in. (0.41 m to 0.36 m), and four vertical elbows of 14 in. (Elbows E1840, E1841, E1843, and E1844). Figure 5 shows the schematic of this pipe.

Figure 6 demonstrates the near wall distributions of liquid fraction along this pipe, while the left part shows the distributions for Elbows E1829, E1830, R1832, E1840, and E1841, and the right part shows the distributions for Elbows E1843 and E1844. As the two-phase mixture passes through these elbows, the centrifugal force governs the liquid droplet behavior and pushes the droplet to the outer side of the elbow, causing a higher liquid fraction (yellow-red region in the plots) to appear there. Special attention is focused on the liquid fraction distribution at vertical Elbow E1841. The downward gravitational force is opposite to the upward centrifugal force within this elbow. The left part of Figure 6 shows more liquid accumulated at the outer side (upper side) of Elbow E1841, which reveals that cen-

trifugal force
two-phase
tal pipe, t
because o
by the fac
the flowin
upper side
The near-v
Elbows E1
effect that
of the elbow
Figure:
distribution

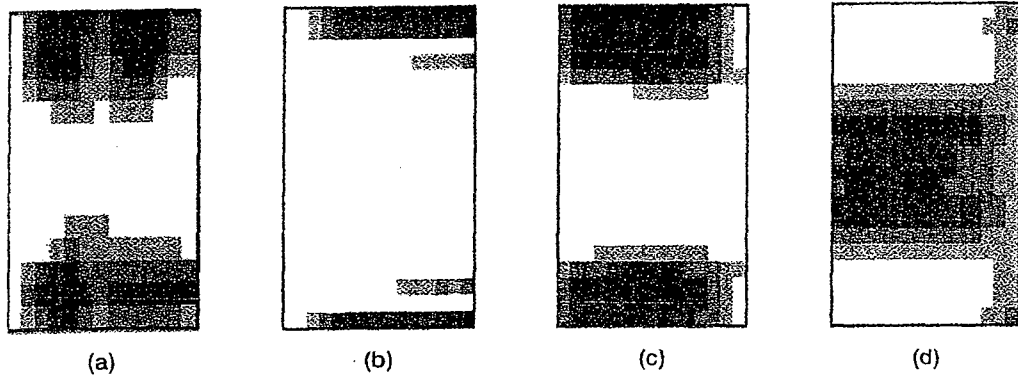


FIGURE 8. Comparison of wear sites for Elbow E1841.

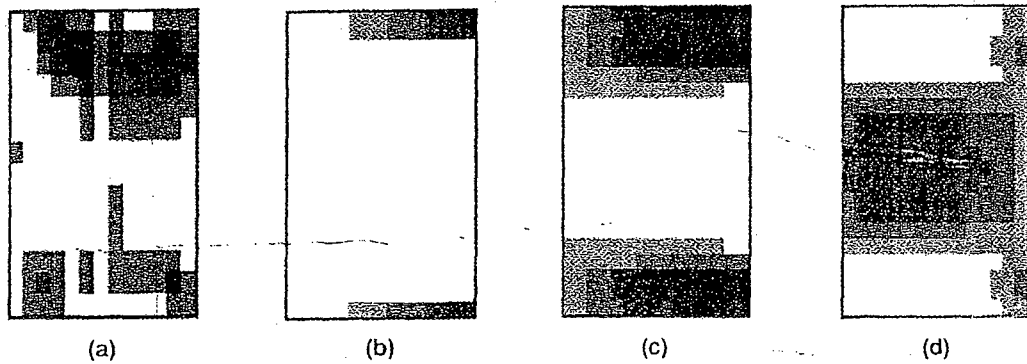


FIGURE 9. Comparison of wear sites for Elbow E1843.

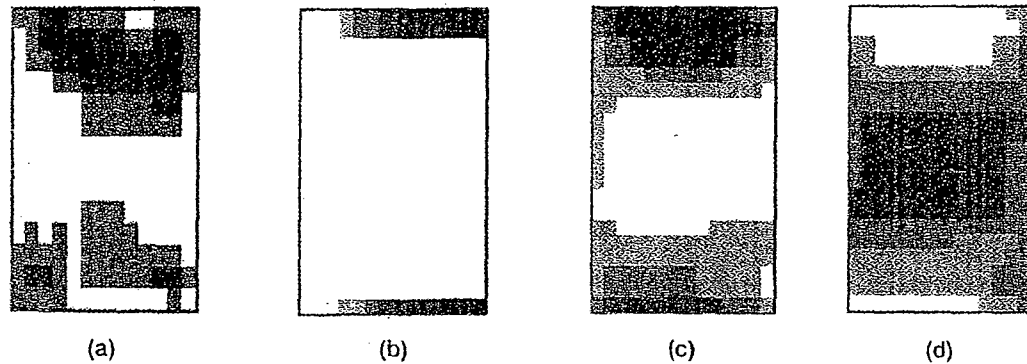


FIGURE 10. Comparison of wear sites for Elbow E1844.

gement
lower
re outer
with the
odel
icen-

image
re
liquid

phase
ynamic
ntinuous
d phase
The
ces on the
asonably
distribu-
clude the
re elbow
down to be
result of
re passes

ation
hemical
olution or
re high-
duction
ement are
t^h wear
of local-
tributions

predicted by the effects of Fe^{2+} production and droplet impingement show satisfactory agreements. These similar wear patterns reveal that these two effects dominate the EC phenomenon for the fittings within the high-quality system.

❖ Since the flow behaviors are not complicated within the elbow, reducer, or expander etc., these parameters (including Fe^{2+} production and droplet

impingement) are proven to be enough to explain the EC phenomenon occurring within these fittings located in the high-quality system.

❖ The next step in the current study will be to simulate the flow characteristics and the related EC phenomenon for T-junctions, within which more sophisticated flow behaviors may occur. Then, additional EC models are needed to capture accurately

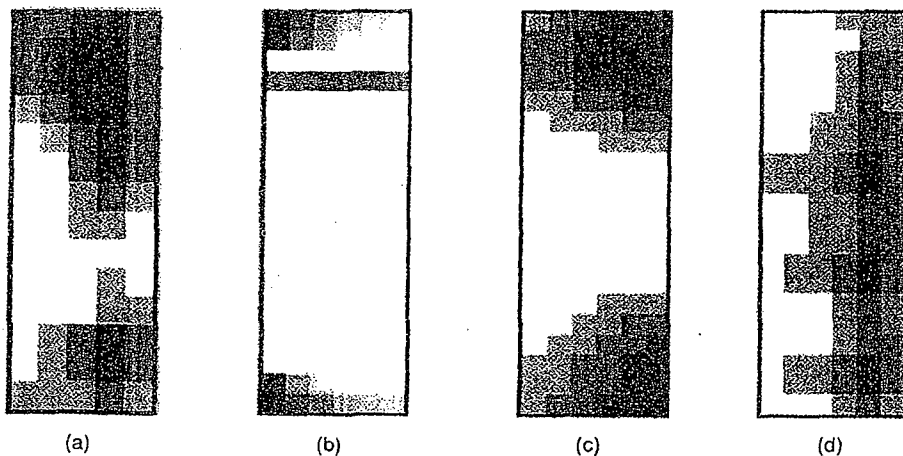


FIGURE 7. Comparison of wear sites for Reducer R1832.

of the outer side in the reducer is located at the upper portion of the two-dimensional plots. In the mean time, Reducer R1832 is a horizontal reducer, and the heavier droplet will be accumulated at the bottom of the pipe because of gravitation, rendering unsymmetrical flow structure and wear pattern. This result is proven in both the measured and predicted wear patterns. This measured result can be captured reasonably by the predicted results using the EC models accounting for droplet impingement (Plot [b]) and Fe^{2+} production (Plot [c]) effects. The satisfactory agreement reveals that these two effects, not the Fe^{2+} transfer effect (Plot [d]), can explain the EC phenomenon occurring within Reducer R1832.

Among this simulated pipe, there are three sets of measured data for Elbows E1841, E1843, and E1844. These three elbows belong to vertical elbows of 90° and are located at the same plane. Similar flow structure and wear pattern within these elbows are expected. The measured distributions of EC locations in these three elbows display similar characteristics, as shown in Plot (a) of Figures 8 through 10. The same results can be simulated by the current local flow model, which includes a three-dimensional, two-fluid model and the appropriate EC models. Comparisons shown in Figures 8 through 10 reveal that Plots (b) and (c) of the predicted wear patterns correspond with Plot (a) of the measured data. The agreement can be explained as the EC phenomena occurring within these elbows are dominated by the effects of droplet impingement and Fe^{2+} production.

Based on the aforementioned description, EC occurring in the high-quality wet steam system can be considered to include the chemical corrosion dominated by Fe^{2+} production and its transfer, and the mechanical erosion mainly contributed by liquid droplet impingement. The EC locations predicted by

the Fe^{2+} production model and droplet impingement model are distributed around the upper and lower parts of the two-dimensional plots, that is, the outer side of the elbows. These distributions agree with the measured data. However, the Fe^{2+} transfer model calculates the serious wear sites that are concentrated at the central part. According to these comparisons of wear patterns, serious EC damage for high-quality wet steam system are governed mostly by the effects of Fe^{2+} production and liquid droplet impingement.

CONCLUSIONS

❖ The complicated three-dimensional, two-phase flow field is obtained by the current hydrodynamic model that treats the vapor phase as the continuous phase and the liquid phase as the dispersed phase because of its high-quality characteristics. The impacts of gravitational and centrifugal forces on the liquid droplet behaviors can be captured reasonably and are shown clearly in plots of near-wall distributions of liquid phase. These phenomena include the droplet being pushed to the outer side of the elbow as a result of centrifugal force and falling down to be accumulated at the bottom of the pipe as a result of gravitational force as the two-phase mixture passes along the horizontal pipe.

❖ The EC phenomenon is a piping degradation mechanism. It essentially consists of the chemical oxidation of carbon steel wall and the dissolution or erosion by flowing fluid. With respect to the high-quality system, the parameters of Fe^{2+} production rate, its transfer rate, and droplet impingement are considered to have profound influence on the wear patterns. Compared to the distributions of EC locations measured by the plant staff, the distributions

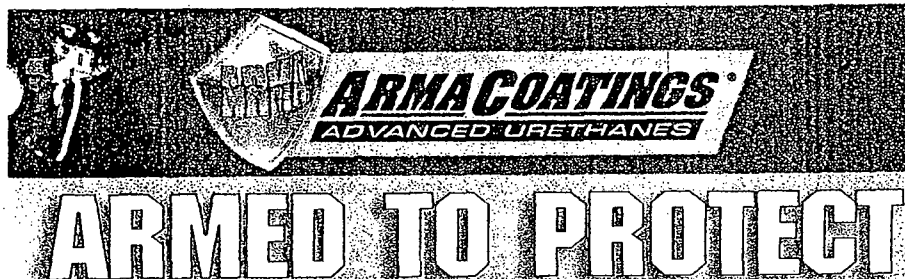
FIG 1
predicted by
let impingem
similar wear
domina
the high
Since the f
within the elt
parameters (u

CORROSION

the wear sites distributed in T-junctions. The current work focused on qualitative prediction of the distributions of EC locations. The quantitative wear rate for a fitting is another worthy topic that will be scheduled for future research.

REFERENCES

1. V.K. Chexal, J.S. Horowitz, "CHEC Computer Program User's Manual," Nuclear Safety Analysis Center (NSAC) 112L, R1, July 1989 (Palo Alto, CA: Electric Power Research Institute, 1989).
2. "CAECE Code, Erosion-Corrosion Mean Prediction for Power Plant Applications," FPI Report FPI-91-255, September 1991.
3. W. Kastner, N. Henzel, B. Stellwag, "Erosion-Corrosion in Power Plants" (Washington, DC: Nuclear Regulatory Commission, 1991).
4. F.N. Remy, M. Bouchacourt, Nucl. Eng. Des. 133 (1992): p. 23-30.
5. P.C. Wu, "Erosion-Corrosion-Induced Pipe Wall Thinning in U.S. Nuclear Power Plants," NUREG-1344 (Washington, DC: Nuclear Regulatory Commission, 1989).
6. J. Postlethwaite, M.H. Dobbin, K. Bergevin, Corrosion 42 (1986): p. 514-421.
7. J. Postlethwaite, U. Lotz, Can. J. Chem. Eng. 66 (1988): p. 75-78.
8. W. Blatt, T. Kohley, U. Lotz, E. Helz, Corrosion 45 (1989): p. 793-803.
9. H. Zeisel, F. Durst, "Computations of Erosion-Corrosion Processes in Separated Two-Phase Flows," CORROSION/90, paper no. 29 (Houston, TX: NACE, 1990).
10. S. Nestic, J. Postlethwaite, Can. J. Chem. Eng. 69 (1991): p. 704.
11. S. Nestic, J. Postlethwaite, Corrosion 47 (1991): p. 582-589.
12. B.E. Launder, D.B. Spalding, Comp. Appl. Mech. Eng. 3 (1972): p. 269.
13. H. Schlichting, Boundary Layer Theory, 7th ed. (New York, NY: McGraw-Hill Book Co., 1978).
14. A.A. Mostafa, H.C. Mongia, Int. J. Heat Mass Transf. 3, 10 (1988): p. 2,063-2,075.
15. R. Clift, J.R. Grace, M.E. Weber, Bubble, Drops, and Particles (New York, NY: Academic Press, 1978).
16. D.B. Spalding, "Modeling a Body-Fitted Coordinate Grid During a PHOENICS Computation," CHAM/PER/88/1 (London, U.K.: Concentration, Heat, and Momentum, Ltd., 1988).
17. D.B. Spalding, "IPSA 1981: New Developments and Computed Results," Imperial College CFDV Report HTS/81/2 (London, U.K.: Imperial College, 1981).
18. S.V. Patankar, D.B. Spalding, Int. J. Heat Mass Transf. 15 (1972): p. 1,787-1,806.
19. S.V. Patankar, "Numerical Heat Transfer and Fluid Flow" (New York, NY: Hemisphere Publishing Corp., 1981).
20. A.D. Gosman, P.J.K. Ideriah, TEACH-2E: A General Computer Program for Two-Dimensional, Turbulent, Recirculating Flow" (London, U.K.: Department of Mechanical Engineering, Imperial College, 1976).
21. "The PHOENICS Beginner's Guide," CHAM/TR100 (London, U.K.: Concentration, Heat, and Momentum, Ltd., 1991).
22. "CDF5-FLOW3D Release 3.3: User Manual" (Oxfordshire, U.K.: Computational Fluid Dynamics Services, 1994).
23. W.T. Sha, B.E. Launder, "A General Model for Turbulent Momentum and Heat Transfer in Liquid Metals" ANL-77-78 (Argonne, IL: Argonne National Laboratory, 1979).



ARMED TO PROTECT

Arm your facility or project for maximum protection against contaminants, chemicals, abrasion or corrosion with Arma Coatings spray-on protective coatings.

Arma Coatings extensive line of polyurethane and polyurea products offer a decisive advantage:

- | | |
|--|--|
| <input type="checkbox"/> Sprays on hot to cure instantly | <input type="checkbox"/> Environmentally safe & friendly |
| <input type="checkbox"/> Minimal down time | <input type="checkbox"/> Can be applied in most environments |
| <input type="checkbox"/> Provides long life durability | <input type="checkbox"/> Offers extreme adhesion |
| <input type="checkbox"/> Highly flexible, permanent seal | <input type="checkbox"/> Can be used for spot application |
| <input type="checkbox"/> 100% solids - no solvents or VOCs | <input type="checkbox"/> Cost effective problem solver |

Applications include, but are not limited to:

- | | |
|--|--|
| <input type="checkbox"/> Containment ponds | <input type="checkbox"/> Clarifiers |
| <input type="checkbox"/> Above and below grade pipes | <input type="checkbox"/> Manhole renovation |
| <input type="checkbox"/> Sludge Hoppers | <input type="checkbox"/> Corrosion resistant containers of all types |
| <input type="checkbox"/> Waste water apparatus | |

For free literature and the dealer in your area, call: **1-800-524-ARMA** or 541-688-3500.

Or visit us on the web: www.armacoatings.com

Dealership opportunities worldwide. Visit our Web site or call for more information.



ABSTRACT

Based
predict
certain n
illuminat
work, i
buffer s
180 W/m
potential
similar
was fou
in the san
nation. Th
same ob
both mat
was expla
the growt
tions indi
white ligh
electric fiel
the electri
cally usef
corrosion or

Submitte
1998.
Center for
Dieke Bide
and Applie
Ravensw
Chemistr
Africa.
Corrosion I
Plata, Arge
UN number
Numbering
Engineers